Interface-Specific Ultrafast Two-Dimensional Vibrational Spectroscopy

JENS BREDENBECK,*,† AVISHEK GHOSH,
HAN-KWANG NIENHUYS, AND MISCHA BONN*

*Fundamental Research on Matter (FOM)–Institute for Atomic and Molecular
Physics, Kruislaan 407, 1098 SJ, Amsterdam, The Netherlands*

RECEIVED ON JANUARY 15, 2009

CONSPECTUS

Surfaces and interfaces are omnipresent in nature. They are not just the place where two bulk media meet. Surfaces and interfaces play key roles in a diversity of fields ranging from heterogeneous catalysis and membrane biology to nanotechnology. They are the site of important dynamical processes, such as transport phenomena, energy transfer, molecular interactions, as well as chemical reactions. Tools to study molecular structure and dynamics that can be applied to the delicate molecular layers at surfaces and interfaces are thus highly desirable.

The advent of multidimensional optical spectroscopies, which are the focus of a special issue of *Accounts of Chemical Research*, and in particular of two-dimensional infrared (2D-IR) spectroscopy has been a breakthrough in the investigation of ultrafast molecular dynamics in bulk media. This Account reviews our recent work extending 2D-IR spectroscopy to make it surface-specific, allowing us to reveal the structure and dynamics of specifically interfacial molecules.

2D-IR spectroscopy provides direct information on the coupling of specific vibrational modes. Coupling between different modes can be resolved and quantified by exciting a particular mode at a specific frequency and probing the effect of the excitation on a different mode at a different frequency. The response is thus measured as a function of two frequencies: the excitation and the probe frequency, which provides a two-dimensional vibrational spectrum. When two vibrational modes are coupled, this will give rise to the intensity in the off-diagonal part of the 2D-IR spectrum. The intensity of the cross-peak is determined by the strength of the coupling between the two modes, which, in turn, is determined by molecular conformation. One can therefore relate the 2D-IR spectrum to the molecular structure. By delaying pump and probe pulses relative to one another, one can obtain additional information about conformational fluctuations.

The surface-specific 2D-IR approach presented here combines the virtues of 2D-IR with the surface specificity and sub-monolayer sensitivity of vibrational sum frequency generation (SFG). We demonstrate its application on a self-assembled monolayer of a primary alcohol on water. It allows for the elucidation of different contributions to the coupling between the different interfacial methyl and methylene stretching modes. Although the surface 2D-IR technique presented here is conceptually closely related to its bulk counterpart, it is shown to have distinct characteristics, owing to the preferential alignment of molecules at the interface and the strict selection rules of the SFG probing scheme. We present an analytic theoretical framework that incorporates these effects and present simulations on instructive examples as well as on the alcohol monolayer. Overall, these results illustrate the potential of extending 2D-IR spectroscopy to the investigation of surface molecular dynamics.
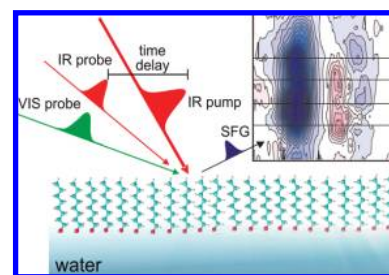
Motivation

Coupling and energy flow through vibrational modes at surfaces and interfaces are important in areas as diverse as heterogeneous catalysis, electrochemistry, and membrane biophysics and chemistry. On the one hand, the coupling of surface vibrational modes is pivotal in determining time scales of energy transfer and surface reaction rates as well as their mechanisms.[1-4] On the other hand, information on surface vibrational coupling can be instrumental in determining (adsorbate) interfacial structure and structural

dynamics. There has therefore been much interest in elucidating details of vibrational coupling at surfaces. Previous surface spectroscopic studies have demonstrated that the effects of delocalization of vibrational energy are apparent in vibrational spectra of metal-adsorbate systems and that combination bands of modes can be observed for strong coupling. Moreover, recent vibrational relaxation studies of interfacial water[5,6] have shown that vibrational energy transfer is very efficient for interfacial water.

It has remained challenging, however, to directly determine vibrational coupling strengths and rates of vibrational energy transfer at surfaces. For molecules in solution, the advent of two-dimensional vibrational spectroscopy has been a breakthrough in elucidating vibrational mode coupling in bulk systems. In two-dimensional infrared (2D-IR) spectroscopy, one vibrational mode A is excited and the effect of this excitation on a different mode B is probed. If the modes are uncoupled, mode B remains unaffected by excitation of mode A and a spectral response is only observed for mode A at identical pump and probe frequencies, i.e., on the diagonal of the 2D-IR spectrum. Inversely, the off-diagonal peaks between modes A and B are determined by the strength of their coupling and depend upon their relative orientation and distance. As such, 2D-IR spectroscopy is increasingly useful in determining molecular structure and dynamics. 2D-IR analogues of 2D-NMR experiments, such as nuclear Overhauser effect spectrometry (NOESY), correlation spectroscopy (COSY), and exchange spectroscopy (EXSY) have been demonstrated;[7−14] we refer to other contributions in this special issue for additional recent examples.

These bulk studies have shown that 2D-IR spectroscopy is capable of resolving structure, structural fluctuations, and structural evolution with femtosecond time resolution of a wide range of systems, from model systems to small peptides and membrane proteins.[7,8,13,15−21] However, measuring vibrational mode coupling at surfaces is challenging, because it requires both distinguishing the signal of a small number of surface molecules from a much larger bulk response and recording this signal within typical vibrational lifetimes (i.e., on sub-picosecond time scales).[22,23]

The focus of this Account is on femtosecond sum frequency generation 2D-IR (SFG-2D-IR) spectroscopy, a 2D-IR spectroscopy with sub-monolayer sensitivity and surface specificity.[24] SFG-2D-IR has been introduced very recently,[24] following theoretical proposals of closely related surface 2D vibrational techniques.[25−27] The experimental approach that we use here is slightly different from the approaches proposed[25−27] and employed[28] previously to elucidate surface intermolecular coupling. Cho proposed two-dimensional infrared-infrared-SFG,[26,27] which was used to determine the intermolecular coupling strength of dipole-coupled CO on a metal surface.[28] Nagata et al. pointed out that this third-order nonlinear optical approach is not inherently surface-specific (only even-order processes are) and proposed surface-specific infrared-infrared-SFG (a second-order nonlinear optical process) as an alternative approach to record surface 2D-IR spectra.[25] The experimental approach that we have developed relies on a fourth-order nonlinear optical process (see, e.g., refs 5 and 6), as will be detailed below.

As a first application of SFG-2D-IR, we investigated a self-assembled monolayer of dodecanol on water, a model system for biological membranes, in the region of the C−H stretching modes of the alkyl chains. Besides these surface 2D spectra, we report additional studies of vibrational dynamics in this system. Moreover, we provide an analytical theoretical framework necessary for the correct interpretation of the surface 2D-IR spectra and illustrate the similarities and differences between bulk and surface 2D-IR spectroscopies.

Experimental Strategy

There exist essentially two ways of doing bulk 2D-IR spectroscopy: in the frequency domain and as a time-domain Fourier transform experiment.[29] We limit ourselves here to the frequency-domain experiment. This is essentially a two-color pump−probe experiment, where a spectrally narrowed [typically $\sim$10−20 cm^{-1} full width at half-maximum (fwhm)], tunable pump pulse selectively excites a specific mode or a specific sub-ensemble of oscillators within a distribution. The femtosecond probe pulse is spectrally broad (typically $\sim$200 cm^{-1} fwhm), allowing us to probe the effect of the pump pulse on a multitude of vibrational modes simultaneously. This process can be described as a sequence of coherent interactions between the sample and the IR laser fields, whereby the third-order coherence is detected, which contains information about vibrational mode coupling and dynamics.[29]

To apply 2D-IR spectroscopy to study vibrational mode coupling at specific surfaces, we introduce an additional interaction with a nonresonant near-IR (800 nm) laser pulse. As shown below, this additional interaction results in monolayer sensitivity and interface specificity. The additional interaction with an optical field effectively upconverts the third-order coherence to an even (fourth)-order coherence, which radiates a field in the visible spectral range, at the sum frequency of near-IR and IR. This upconversion process is beneficial in two ways. First, it ensures surface specificity; as for centrosym-
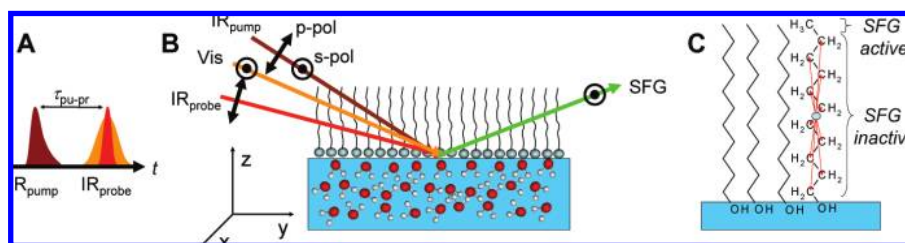
FIGURE 1. (A) SFG-2D-IR pulse sequence. (B) Sample configuration and coordinate system. Three pulses are incident in the *yz* plane. A spectrally narrowed (temporally long) intense infrared pump pulse excites a specific vibration at the interface. A transient SFG spectrum is recorded by mixing a femtosecond infrared probe pulse with a picosecond visible pulse at the interface. Polarizations of the different pulses are indicated in the graph. (C) SFG active methyl and inactive methylene groups of the self-assembled monolayer. Methylene groups are SFG-inactive because of the presence of a center of inversion in the alkyl chain.

metric materials, an even-order response can only originate from the surface molecules. This selection rule underlies the processes of surface second-harmonic generation (SHG) and surface sum-frequency generation (SFG). Second, the upconverted signal is background-free and lies in the visible spectral range, where charge-coupled device (CCD) cameras with high quantum efficiencies are available, readily providing submonolayer sensitivity.

We designed our SFG-2D-IR experiment as an IR-pump−SFG-probe five-wave mixing scheme (Figure 1),[5,30,31] in analogy to the pump−probe scheme used in bulk 2D-IR spectroscopy.[29] Details of the setup can be found in ref 32. Briefly, tunable, high-energy mid-IR pump pulses (tunable, around 2900 cm^{-1}; width, 180 cm^{-1} fwhm; duration, 100 fs fwhm; pulse energy, up to 90 μJ) are generated by parametric conversion. From a part if this pulse, a tunable, narrowband IR-pump pulse (duration, 900 fs; 20 cm^{-1} fwhm, bandwidth) is generated using a computer-controlled Fabry−Perot interferometer, to excite the sample surface. The tunable central frequency of the pump determines the vertical axis of the 2D vibrational spectrum. The horizontal axis is determined by the infrared probe frequency; the pump-induced changes in the surface vibrational response are probed after a delay τ_{pu-pr} by a broadband IR probe pulse (120 fs, 180 cm^{-1} bandwidth) and a narrowband 800 nm probe pulse (3 ps, 12 cm^{-1} bandwidth, determining the resolution along the probe axis). The probe pulse pair interacts with the sample surface to radiate a signal at the sum frequency of the 800 nm pulse and the frequency of the vibrations that are resonant with the IR-probe pulse. The SFG-2D-IR signal is spectrally resolved with a spectrograph and a CCD camera. In the experiment, the pump frequency is scanned and the SFG-2D-IR signal is plotted as a function of pump and probe frequencies in a two-dimensional spectrum. The difference spectrum reveals the effect of the pump pulse on all resonances within the probe bandwidth. The IR pump, probe, and vis probe beams lie in a vertical plane and have incident

angles of 46°/50°/56°, respectively, with respect to the surface normal. The polarizations for the SFG/vis/IR beams were controlled using $\lambda/2$ plates and were s/s/p in all experiments; the polarization of the pump pulse was varied between s and p.

1-Dodecanol (Sigma Aldrich) and D$_2$O (99.96 atom % D, Cambridge Isotopes) were used without further purification. A self-assembled monolayer of 1-dodecanol was prepared by bringing a grain of 1-dodecanol in contact with the D$_2$O surface. To avoid laser heating and resulting damage of the sample, the sample trough was rotated. The vertical sample position was controlled by a feedback loop to compensate for evaporation.[32]

SFG-2D-IR of a Self-Assembled Monolayer

Panels c and d of Figure 2 show the SFG-2D-IR spectra of the dodecanol monolayer on D$_2$O for p and s polarization of the IR pump pulse.[39] The 2D data in Figure 2 are difference spectra, i.e., SFG intensity difference with and without vibrational excitation pulse. In the measurements, the difference SFG spectra are recorded at different pump frequencies, so that the 2D spectrum is constructed from horizontal traces. Blue (red) denotes a pump-induced decrease (increase) of SFG intensity. Along the probe axis, we depict the static 1D SFG spectrum of the monolayer (Figure 2b). The two bands in the SFG spectrum can be assigned to the symmetric CH$_3$ stretch vibration of the dodecanol methyl group being split by a Fermi resonance with an overtone of a bending mode to give two peaks [CH$_3$(ss) at 2873 cm^{-1} and CH$_3$ (ss)$_{FR}$ at 2935 cm^{-1}].[33−35] A contribution of the asymmetric stretch CH$_3$(as) at 2950 cm^{-1} [35] is not clearly resolved.

Panels c and d of Figure 2 show the SFG-2D-IR spectra of the self-assembled monolayer at τ_{pu-pr} = 700 fs. In addition to the diagonal peaks, several off-diagonal peaks appear as expected in analogy to bulk 2D-IR spectroscopy. The interfacial molecular alignment allows us to enhance the sensitivity
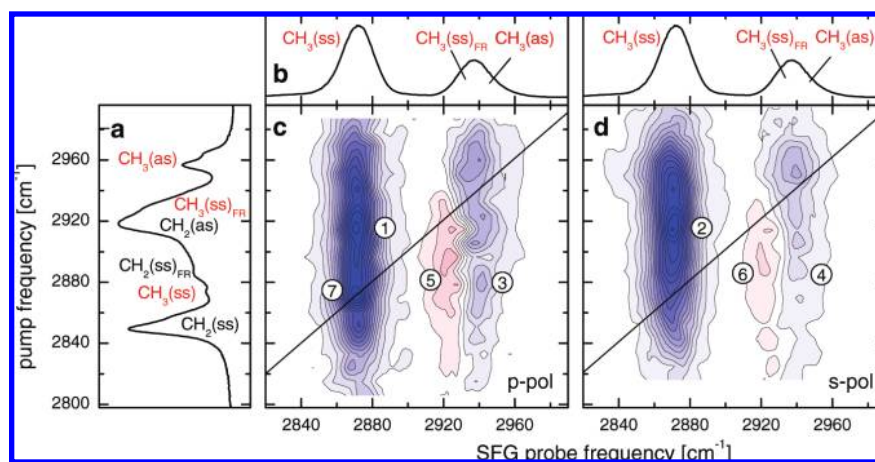
FIGURE 2. SFG-2D-IR spectra of a dodecanol monolayer on water. Blue (red) denotes a pump-induced decrease (increase) in SFG intensity. (a) IR spectrum of crystalline dodecanol at 150 K. (b) SFG spectrum of the monolayer. (c) SFG-2D-IR spectrum, with p-polarized pump, $t = 0.7$ ps. (d) SFG-2D-IR spectrum, with s-polarized pump, $t = 0.7$ ps. The lines indicate the diagonal, and the numbers correspond to features discussed in the text. Modes assigned in red are both IR- and SFG-active.

to specific modes by controlling the polarization of the pump laser pulse, as evident from a comparison of panels c and d of Figure 2.

Two striking characteristic of the new technique are apparent from the data when comparing the surface SFG-2D-IR technique to bulk 2D-IR spectroscopy. First, the regions of high intensity are mostly oriented vertically in the spectra, as opposed to conventional 2D-IR, where most intensity generally lies along the diagonal. This is a result of having different selection rules for pump and probe interactions. The SFG probe selection rules require IR and Raman activity and appropriate symmetry breaking. This renders the CH_2 modes SFG-inactive for ordered alkyl chains, because there is a center of inversion symmetry along the alkyl chain (Figure 1c). The pump selection rule only requires infrared activity of the vibrational mode, so that all infrared active CH_2 and CH_3 modes can be excited. Hence, we plot the IR absorption spectrum of (bulk crystalline) dodecanol along the pump axis (Figure 2a). The IR absorption features in Figure 2a are assigned to symmetric and antisymmetric CH_2 and CH_3 stretching vibrations (denoted ss and as in the following), split by Fermi resonances (denoted FR) with C—H bending modes of the according symmetry.[33–35]

As a result of the different selection rules, no cross-peaks can appear at CH_2 mode frequencies (unless the symmetry is broken by the pump pulse; see below). It is clear from panels c and d of Figure 2 that the coupling between CH_2 and CH_3 modes is sufficiently strong, so that excitation of the CH_2 modes is apparent at CH_3 mode frequencies. The fact that the high-intensity regions are mostly aligned vertically in the spectra can be understood by noting that the effect of the pump will primarily be detected at the two SFG-active CH_3 modes

shown in Figure 2b. Some of the off-diagonal peaks (such as peaks 1 and 2 in panels c and d of Figure 2 are remarkably strong.

A second striking observation is that the SFG-2D-IR spectra are dominated by decreases in the SFG intensity (blue), with remarkably little increase in SFG-2D-IR intensity (positive red features in panels c and d of Figure 2). In bulk 2D-IR spectroscopy, an individual 2D-IR spectral response usually consists of a positive and negative feature because of ground-state depletion and excited-state absorption. The latter contribution is largely suppressed in SFG-2D-IR spectra, owing to the relative insensitivity of SFG to excited-state transitions, as will be shown below.

To complement the SFG-2D-IR experiments, we collected broadband IR-pump−SFG-probe spectra to investigate the vibrational dynamics of the CH stretch modes. Figure 3 shows the result of broadband IR-pump−SFG-probe experiments on a dodecanol monolayer. For these experiments, the Fabry−Perot filter was removed from the pump beam path. The resulting vibrational relaxation times are very similar to those reported for the C−H modes of various lipid monolayers.[30] Panels a and b of Figure 3 show the response of the $CH_3(ss)$ and $CH_3(ss)_{FR}$ peak in the dodecanol SFG spectrum (Figure 2b) to a broadband pump pulse. Owing to the collective alignment of methyl groups at the interface, p-polarized pump light provides more efficient CH_3 excitation than s-polarized light. The vibrational lifetime of $CH_3(ss)$ is found to be $T_1 = 7 \pm 0.5$ ps, and the lifetime of $CH_3(ss)_{FR}$ is $T_1 = 1.5 \pm 0.4$ ps. Panels c and d of Figure 3 show the effect of s-polarized excitation. In comparison to p polarization, a delayed signal ingrowth is observed, with the signal peaking at about $\tau_{pu−pr} = 1$ ps, also analogous to recently obtained results for lip-
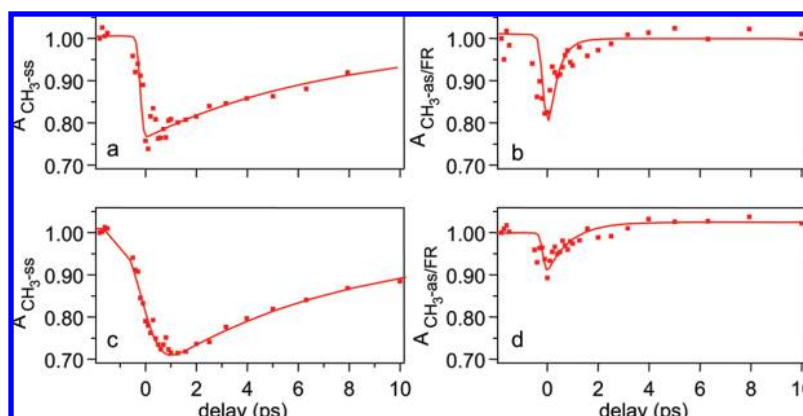
FIGURE 3. Results of broadband SFG pump−probe spectroscopy on dodecanol monolayers on water. Plotted are the amplitudes of the contributions to the second-order nonlinear susceptibility from the different modes (see eq 4), obtained from fits to transient SFG spectra at different pump−probe delay times. (a) $CH_3(ss)$, p-polarized pump. (b) $CH_3(ss)_{FR}$, p-polarized pump. (c) $CH_3(ss)$, s-polarized pump. (d) $CH_3(ss)_{FR}$, s-polarized pump.

ids.[30] This effect was attributed to the fact that the s-polarized pump pulse excites the in-plane CH_2 vibrations more efficiently that relax rapidly ($T_1 = 0.8$ ps), leading to a population of low-frequency modes that anharmonically couple to the CH_3 modes, thereby increasing the observed signal as CH_2 relaxation proceeds.[30] This type of incoherent energy transfer or local heating will also contribute to cross-peaks in the 2D spectra between CH_2 and CH_3 modes, such as cross-peak 1 in Figure 2c. In contrast to direct anharmonic coupling between the high-frequency modes, which is instantaneous, the energy transfer via low-frequency modes will generate a time-dependent contribution.

Theoretical Background

In surface 2D-SFG spectroscopy, fields E at two different frequencies ω_{IR} and ω_{VIS} are mixed at the sample surface to generate a third sum-frequency field at a frequency $\omega_{SF} = \omega_{IR} + \omega_{VIS}$ (Figure 1)

$$E_i^{SF}(\omega_{IR} + \omega_{VIS}) \propto \sum_{jk} \chi_{ijk}^{(2)} E_j^{VIS} E_k^{IR}(\omega_{IR}) \quad (1)$$

where $\chi_{ijk}^{(2)}$ are the components of the third-rank second-order nonlinear-susceptibility tensor $\chi^{(2)}(\omega_{IR})$, which here is mostly independent of ω_{VIS} because the latter is chosen to be not resonant with transitions in the molecule. Owing to the vibrational resonance, $\chi^{(2)}$ is a complex-valued quantity. In a centrosymmetric (bulk) system, $\chi^{(2)}$ is generally negligibly small. However, at the liquid surface, where the symmetry is broken and molecules have a preferential orientation, $\chi^{(2)}$ is nonzero. The SFG signal therefore originates from surface molecules, and its magnitude is related to the type of molecules and their orientational distribution. In the dodecanol−water system, most of the SFG signal originates from resonances of

the C−H stretch vibrations of the terminal CH_3 group in the dodecanol molecules. Contributions from different vibrational resonances add up to generate the overall SFG field and may interfere both destructively or constructively.

In the SFG-2D-IR experiments discussed in this paper, the nonlinear susceptibility $\chi^{(2)}(\omega)$ is modified by a narrowband pump pulse at frequency ω_{pu}. This fourth-order process is modeled here in terms of a non-equilibrium time-dependent second-order susceptibility. While this description neglects time orders where the probe interaction precedes one or both of the pump interactions, it is expected to give a good representation of the spectral features occurring in SFG-2D-IR spectra for the experimental conditions used here.[22] The SFG-2D-IR signals in Figure 2 are the difference in intensity of SFG spectra recorded in the presence and absence of the IR pump (pu) pulse

$$\Delta I^{SF}(\omega_{pu}, \omega_{pr}) = I_{pump}^{SF}(\omega_{pu}, \omega_{pr}) - I_0^{SF}(\omega_{pr}) \quad (2)$$

$$\propto |\chi_{pu}^{(2)}(\omega_{pu}, \omega_{pr})|^2 - |\chi_0^{(2)}(\omega_{pr})|^2 \quad (3)$$

where $\chi^{(2)}$ is the scalar effective nonlinear susceptibility for a given combination of probe and SFG polarization angles.

In the steady state (i.e., without pump), assuming homogeneously broadened lines, one may write

$$\chi_0^{(2)}(\omega_{pr}) = \sum_n \frac{A_n}{\omega_{pr} - \omega_n + i\Gamma_n} \quad (4)$$

where ω_n is the resonance frequency of a transition n with line width Γ_n and A_n is an amplitude factor that accounts for the surface density of molecules, their orientational distribution, and IR and Raman scattering cross-sections. Note that the sign of A_n is related to the absolute orientation of the interfacial transition dipole moment (i.e., pointing up or down).

After excitation, the nonlinear susceptibility $\chi_{pu}^{(2)}$ is affected in several ways. First, a reduction of $\chi^{(2)}$ because of bleach and stimulated emission (B,SE) occurs at probe frequencies corresponding to excited $0-1$ transitions, while an increase because of excited-state absorption (EA) occurs at the corresponding $1-2$ transitions. Second, an excitation of mode n can cause the transition frequency for another mode m to change because of anharmonic coupling. Finally, the IR pump affects different tensor components differently because the azimuthal symmetry is broken after the linearly polarized pump pulse preferentially excites vibrational modes with a dipole moment along the pump field. For example, for the geometry of Figure 2, excitation of the CH$_3$(ss) mode with a p-polarized pump creates a nonzero $\chi_{xxy}^{(2)}$ component (see the Supporting Information and ref 36). The time evolution of these tensor elements will be affected by vibrational relaxation and reorientational motion of surface molecules. For dodecanol, reorientation will not affect the dynamics of Figure 3, because no significant reorientation in the quasi-crystalline monolayer is expected on the picosecond time scale of the experiment. We neglect this effect in our analysis.

We first define $N_n(\omega_{pu})$ as the fraction of molecules where mode n is excited for a given pump frequency

$$N_n(\omega_{pu}) = D_n \int I^{pu}(\omega)\alpha_n(\omega)d\omega \qquad (5)$$

where $I^{pu}(\omega)$ is the pump spectrum, $\alpha_n(\omega)$ is the absorption cross-section of transition n, and D_n is a prefactor that accounts for orientation effects and the polarizations of the pump pulse (see the Supporting Information). The B,SE contribution to $\chi^{(2)}$ is

$$\chi_{B,SE}^{(2)}(\omega_{pu}, \omega_{pr}) = \sum_n \frac{A_n[N_{gs}(\omega_{pu}) - N_n(\omega_{pu})]}{\omega_{pr} - \omega_n + i\Gamma_n} \qquad (6)$$

where

$$N_{gs}(\omega_{pu}) = 1 - \sum_n N_n(\omega_{pu}) \qquad (7)$$

represents the number of unexcited (ground-state) molecules. We assume that the pump intensity is sufficiently low and that at most one mode is excited in a single molecule. The excited-state contribution to $\chi^{(2)}$ reads

$$\chi_{EA}^{(2)}(\omega_{pu}, \omega_{pr}) = \sum_{n,m} \frac{\sigma_{nm}A_nN_n(\omega_{pu})}{\omega_{pr} - \omega_n + \Omega_{nm} + i\Gamma_n} \qquad (8)$$

where Ω_{nm} is the anharmonicity and σ_{nm} accounts for differences in transition dipole moments. For harmonic oscillators

$$\sigma_{nm} = \begin{cases} 2 & (n = m) \\ 1 & (n \neq m) \end{cases} \qquad (9)$$

which is a good approximation for the relatively small anharmonicities in the dodecanol system. The total effective nonlinear susceptibility is

$$\chi_{pu}^{(2)}(\omega_{pu}, \omega_{pr}) = \chi_{B,SE}^{(2)}(\omega_{pu}, \omega_{pr}) + \chi_{EA}^{(2)}(\omega_{pu}, \omega_{pr}) \qquad (10)$$

If $\Omega_{nn} = 0$, the B,SE contributions would be canceled by the corresponding EA contributions, which would result in the absence of diagonal peaks in the 2D spectrum. Furthermore, off-diagonal (cross) peaks will only appear in the 2D spectrum for mode combinations for which $\Omega_{nm} \neq 0$.

Specific Characteristics of the 2D-IR Surface Implementation

Upon inspection of the SFG-2D-IR spectra in Figure 2, a first striking observation is that the intensity of the 2D spectrum is largely aligned vertically, along the pump axis. This contrasts with conventional 2D-IR spectra, where the predominant response lies along the diagonal. As explained above, this is caused by the different selection rules for the excitation (IR) and probing (SFG) processes, which means that different steady-state spectra should be considered. For the pump, an additional subtlety exists: owing to the alignment of the dodecanol molecules on the surface, the interaction strength of the pump with specific modes depends upon the relative orientation of the pump polarization with the transition dipole moment of the relevant mode. One has to take into account, in addition to the absorption cross-section, the relative excitation density dictated by orientational effects, sample geometry, and Fresnel factors (see the Supporting Information). The relative pumping efficiency of CH$_3$(ss) versus CH$_2$(as) is 4 times bigger for the p-polarized pump (Figure 2c) compared to the s-polarized pump (Figure 2d) (see the Supporting Information). This leads to the pronounced appearance of the CH$_3$(ss) diagonal peak in position 7 in Figure 2c.

A second feature in the SFG-2D-IR spectra in Figure 2 that set it apart from conventional 2D-IR spectra is the relative lack of SFG signal increases; in bulk 2D-IR spectroscopy, a positive feature is always accompanied by an equally large negative feature, owing to the simultaneous ground-state depletion and excited-state absorption. This can be explained by noting the relative insensitivity of SFG toward excited-state transitions: the SFG signal intensity is proportional to the *square* of the nonlinear susceptibility $\chi^{(2)}$, which, in turn, is proportional to the population difference ΔN^2 of the levels involved in a transition. For a system with only a single vibrational mode and 10% excitation ($N_1 = 0.1$), the SFG signal
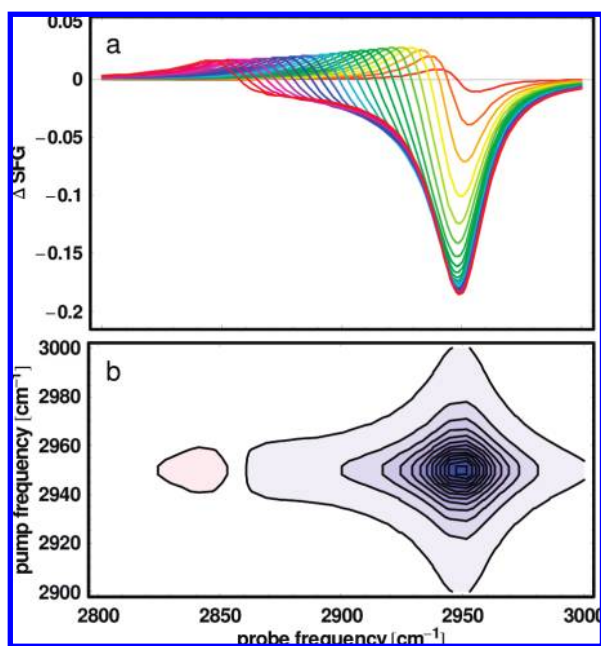
FIGURE 4. Simulated SFG-2D-IR response of a single anharmonic oscillator. (a) Cuts through the 2D spectrum for $\omega_{pu} = 2950$ cm^{-1} and $\Omega = 2, 6,..., 98$ cm^{-1}. (b) Full SFG-2D-IR spectrum for $\Omega = 98$ cm^{-1}.

changes will have a ratio $\Delta I_{B,SE}^{SF}/\Delta I_{EA}^{SF} = 0.36:0.04$, i.e., in a ratio of 9:1 rather than 1:1, where a twice larger IR cross-section has been assumed for the excited state.

Given these considerations, it is in fact somewhat surprising to see the relatively intense positive (red) peaks in the SFG-2D-IR spectra (positions 5 and 6 in Figure 2). This can be explained by noting that the SFG field contributions from different modes can interfere both constructively or destructively. Taking into account the complex-valued nature of the nonlinear susceptibility, we can write

$$|\chi_{pu}^{(2)}|^2 = |\chi_{B,SE}^{(2)}|^2 + |\chi_{EA}^{(2)}|^2 + 2\mathscr{R}(\chi_{B,SE}^{(2)}\chi_{EA}^{(2)}) \qquad (11)$$

In addition to the square contributions, we obtain an interference term of bleach and stimulated emission at $v = (0 \rightarrow 1)$ with excited-state absorption at $v = (1 \rightarrow 2)$. In other words, the overtone contribution is heterodyned by the fundamental.

To illustrate the effect of coherent mixing of different sources of SFG signal from the interface, we consider a few simplified cases in the following. Figure 4 shows a simulated SFG-2D-IR spectrum of a single transition for different anharmonicities. It is evident from Figure 4a, which shows cuts through the 2D spectrum along the main horizontal, that the relative contribution of the $v(1 \rightarrow 2)$ transition decreases as the self-anharmonicity increases. This is the result of a decreasing degree of heterodyning between $v(0 \rightarrow 1)$ and $v(1 \rightarrow 2)$ as the frequency difference increases; a very different ratio of
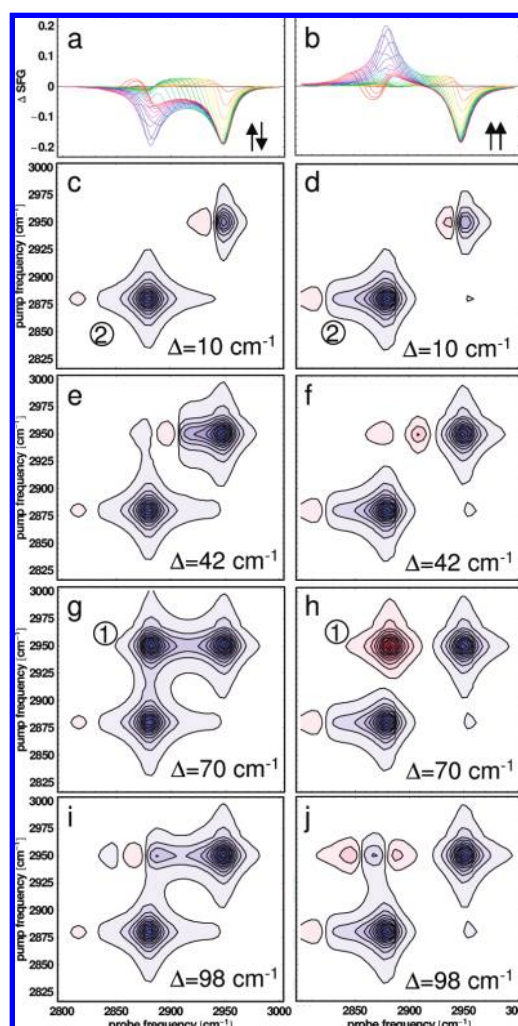

FIGURE 5. Simulated SFG-2D-IR response of two *uncoupled* anharmonic oscillators. (a and b) Cuts through the 2D spectra for $\omega_{pu} = 2950$ cm^{-1} and varying $\Omega = 2, 6,..., 98$ cm^{-1} for the high-frequency oscillator. The transition dipoles point in (a) opposite or (b) the same direction. (c−j) SFG-2D-IR spectra for various Ω of the high-frequency oscillator with (c, e, g, and i) opposite or (d, f, h, and j) the same direction of the transition dipoles. All spectra are on the same scale.

the amplitudes of the two contributions can be observed, depending upon their frequency separation.

For precisely the same reason, the interference between fields originating from different oscillators can lead to unexpected amplification of the otherwise weak excited-state absorption. Figure 5 shows the situation for two *uncoupled* oscillators, where the anharmonicity Ω of the high-frequency oscillator is varied. With increasing Ω, the excited-state absorption contribution of the high-frequency oscillator shifts toward the frequency of the low-frequency oscillator, leading to interference. As can be seen in position 1 in panels g and h of Figure 5, the interference can result in strong cross-peaks, even in the absence of anharmonic coupling between the oscilla-

tors. This is true for oscillators with parallel (column below Figure 5a) and antiparallel (column below Figure 5b) orientation of transition dipoles. However, the sign of the interference critically depends upon the relative sign of the two interfering $\chi^{(2)}$ values. When the dipoles are antiparallel, the emitted interfering wave experiences a 180° phase shift, leading to a flip in the sign of the interference (position 1 in panels g and h of Figure 5). This provides very direct information on the relative orientation of transition dipoles and might prove very useful for future applications. The change in the shape of the low-frequency peak with the change in its transition dipole orientation (position 2 in panels c and d of Figure 5) is a result of the interference with the high-frequency oscillator as well.

Although the interference of coherent polarizations from different sources can lead to off-diagonal peaks that are unrelated to vibrational coupling, the presence of true coupling gives rise to other features in the 2D spectrum that can unequivocally be associated with that coupling. This is illustrated in Figure 6, which shows the same two resonances as in Figure 5, however, with an off-diagonal anharmonicity of $\Omega_{1,2} = 8$ cm^{-1} representing coupling. It is evident that the cross-peak in the lower right corner, at $\omega_{pr} = 2950$ cm^{-1} and $\omega_{pu} = 2875$ cm^{-1} (position 1 in Figure 6) is present, independent of the degree of interference, and provides a good marker of the coupling strength. It is absent for the uncoupled case shown in Figure 5.

We summarize the main differences between the 2D-SFG technique presented here and the more conventional 2D-IR approach in Table 1.

The question then rises whether, for the dodecanol SFG-2D-IR spectra (Figure 2), the positive contributions (positions 5 and 6) are interference effects or the result of anharmonic coupling. The CH$_3$(ss) and CH$_3$(ss)$_{FR}$ modes have the same sign, which upon a pump-induced decrease of the CH$_3$(ss) band would indeed lead to a positive/negative feature on CH$_3$(ss)$_{FR}$ (in the case of an opposite sign, it would be negative/positive). However, in the case of interference, the modulation on the CH$_3$(ss)$_{FR}$ band should follow directly the pump-induced changes of the CH$_3$(ss). This is not the case, and furthermore, the positive contribution is stronger than expected for pure interference. We therefore can conclude that other mechanisms play a role.

Two mechanisms may be noted: one is the generation of cross-peaks because of anharmonic coupling, either between the high-frequency modes or between CH3(ss)$_{FR}$ and low-frequency modes populated after population relaxation. A second mechanism that could lead to a pump-induced increase of SFG is pump-induced symmetry breaking, which would
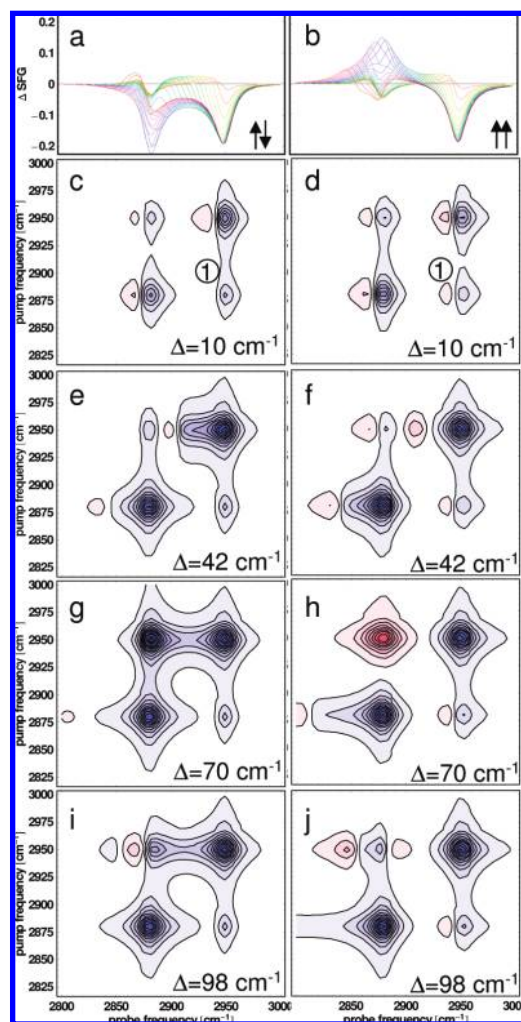

FIGURE 6. Simulated SFG-2D-IR response of two coupled anharmonic oscillators. The off-diagonal anharmonicity is $\Omega_{1,2} = 8$ cm^{-1}. (a and b) Cuts through the 2D spectra for $\omega_{pu} = 2950$ cm^{-1} and varying $\Omega = 2, 6,..., 98$ cm^{-1} for both oscillators simultaneously. The transition dipoles point in (a) opposite or (b) the same direction. (c−j) SFG-2D-IR spectra for various Ω with (c, e, g, and i) opposite or (d, f, h, and j) the same direction of the transition dipoles. All spectra are on the same scale.

cause additional nonzero tensor elements for SFG (see the Supporting Information).

On the basis of the experimental 1D spectra, the absorption spectrum (Figure 2a) and the static SFG spectrum (Figure 2b), we can now attempt a simulation of the SFG-2D-IR response using the theoretical framework introduced above. In the simulation, we do not explicitly consider pump-induced symmetry breaking (see the Supporting Information).

Figure 7 shows such a simulation. As input for the simulation, we used fits to the experimental SFG and IR spectra. Panels c and d of Figure 7 show the fit to the static SFG spectrum; panels a and b of Figure 7 depict the fits to the absorption spectrum, corrected for the polarization-dependent IR cross-

TABLE 1. Comparison of Surface and Bulk 2D-IR

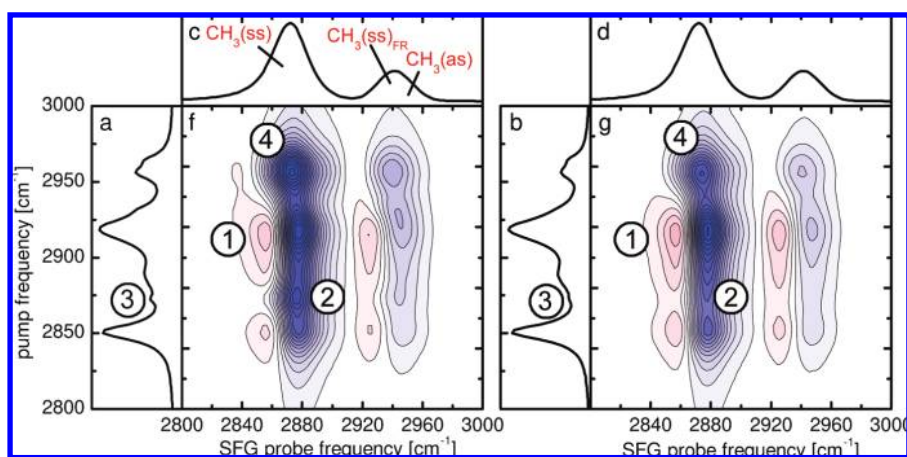| SFG-2D-IR	2D-IR
fourth order in the field: $P_{2D-SFG} = \chi^{(4)} E_{IR}^{pump} E_{IR}^{pump} E_{IR}^{probe} E_{VIS}$	third order in the field: $P_{2D-IR} = \chi^{(3)} E_{IR}^{pump} E_{IR}^{pump} E_{IR}^{probe}$
surface specific	bulk sensitive
different selection rules on the pump and probe axes	same selection rules on the pump and probe axes
pronounced polarization dependence because of surface alignment	sample typically isotropic
background-free detection in the visible spectral range	detection in the IR spectral range
coherent interaction of different source terms	isotropic orientation scrambles the phase
square dependence on oscillators density (linearized by heterodyning)	linear dependence on oscillators density

section of the surface layer. For the normalized spectra shown in panels a and b of Figure 7, the result of varying the IR pump polarization may seem subtle but the variation of exciting the CH_3 mode is apparent at position 3 in panels a and b of Figure 7. The resulting 2D-SFG spectrum was obtained using a diagonal anharmonicity of $\Omega_{n,n} = 60$ cm^{-1} for the C−H oscillators, off-diagonal anharmonicities of $\Omega_{n,m} = 25$ cm^{-1} for C−H oscillators sharing a C atom, and $\Omega_{n,m} = 5$ cm^{-1} for the other C−H oscillators.

The 2D simulation gives a good representation of the main features of the experimental spectra. The most obvious difference compared to the experiment is the positive SFG intensity observed at the low-frequency side of the $CH_3(ss)$ band (position 1 in panels f and g of Figure 7). This can be readily explained by the fact that the simulation used a Gaussian IR probe spectrum, while the experimental spectrum fell off more quickly then Gaussian, leading to a rapidly decreasing amplitude of the SFG signal for $\omega < 2860$ cm^{-1}. Nevertheless, we decided to show the positive contribution here for completeness. The polarization dependence of the $CH_3(ss)$ diagonal peak (position 2 in panels f and g of Figure 7) is reproduced well, being a consequence of the difference of excitation efficiency of the oriented CH_3 group as reflected by the polarization-corrected IR cross-sections (position 3 in panels a and b of Figure 7). We observe relatively strong off-diagonal intensity at position 4, between the $CH_3(ss)$ and the $CH_3(as)$ peaks,

resembling the situation in the experiment. According to the simulation, this is caused by interference between fundamental and excited-state contributions as discussed in the context of Figure 5g.

We would like to note that the values that we used for the off-diagonal anharmonicities of $\Omega_{n,m} = 25$ cm^{-1} for C−H oscillators sharing a C atom and $\Omega_{n,m} = 5$ cm^{-1} for the other C−H oscillators to obtain reasonable correspondence with the experiment appear to be reasonable numbers but are effective coupling coefficients that should be considered with some caution. These single numbers contain contributions from direct anharmonic coupling but also from potential (indirect) symmetry breaking (see the Supporting Information) and from indirect anharmonic coupling. The fact that the latter effect may play a role is evident from the dynamics traces in Figure 3, which demonstrate that some of the relaxation processes occur on time scales very similar to the pump−probe delay time of 700 fs. As a result, low-frequency modes that are excited upon vibrational relaxation may affect the 2D-SFG spectra as well.

In the future, the interpretation of the experimental data could be greatly simplified if in addition a detection scheme complementary to that presented here was used; i.e., if the SFG signal were to be detected in a heterodyne fashion, by mixing in an independently generated local oscillator signal at the SFG frequency (as demonstrated recently for static SFG

FIGURE 7. SFG-2D-IR simulation based on the experimental absorption spectrum and the steady-state SFG spectrum.

spectroscopy[37,38]), the response would become linear rather than quadratic in the excitation density at both the ground- and excited-state transitions. Effects in the spectrum because of self-heterodyning of single oscillators would also be lifted, and all off-diagonal intensity would be traceable directly to vibrational coupling, in analogy to conventional 2D-IR spectroscopy.

Conclusion and Outlook

In summary, we have discussed the implementation of ultrafast surface 2D-IR SFG spectroscopy. This technique shows great promise for a variety of applications, including the study of the structure and reactivity of (mixed) molecular adsorbate layers in catalytic systems, the structures and interactions of membranes and membrane proteins, as well as the structure and dynamics of interfacial water in various systems. We have presented here a complete analytical theory of surface 2D-IR SFG spectroscopy and have demonstrated that heterodyne detection of the 2D SFG signals will further facilitate the interpretation of the experimental results in terms of interfacial vibrational coupling.

Supporting Information Available. Polarization dependence of the IR cross-section at the surface, Fresnel correction, and pump-induced symmetry breaking. This material is available free of charge via the Internet at http://pubs.acs.org.

BIOGRAPHICAL INFORMATION

Jens Bredenbeck was born in 1975 in Osnabrück, Germany. He obtained his diploma in chemistry in 2000 under the guidance of Reinhard Schinke, Max Planck Institute for Flow Research, Göttingen. He joined Peter Hamm′s group at the Max Born Institute of Nonlinear Optics in Berlin and completed his Ph.D. in 2005 at the University of Zurich. After postdoctoral stays in Zurich and with Mischa Bonn at AMOLF, Amsterdam, he received the Sofja-Kovalevskaja Award of the Alexander von Humboldt-Foundation and started his group at the University of Frankfurt in 2007. In 2007, he was elected Adjunct Investigator of the Cluster of Excellence ″Macromolecular Complexes″. His research program explores molecular structure and dynamics over a wide range of time scales as well as the development of nonlinear vibrational spectroscopies.

Avishek Ghosh was born in 1979 in London, U.K. He received his B.Sc. (honors) degree in 2001 from St. Stephen, his M.Sc. in chemistry from the Indian Institute of Technology, Delhi (India). He is finishing his Ph.D. in chemistry at the FOM−Institute for Atomic and Molecular Physics (AMOLF) and Leiden University under his advisor, Prof. Mischa Bonn. His research interests include nonlinear optics, ultrafast spectroscopy, surface science, and biophysics.

Han-Kwang Nienhuys was born in 1973 in Utrecht, The Netherlands, and received a Ph.D. in 2002 on the subject of time-resolved mid-infrared spectroscopy of water at the Technical University of Eindhoven (Prof. Rutger A. van Santen and Huib J. Bakker). He subsequently stayed as a postdoc with Prof. Villy Sundström at the University of Lund, Sweden, working on time-resolved terahertz spectroscopy and then on various subjects related to ultrafast spectroscopy at AMOLF. In 2009, he moved to the semiconductor company ASML in The Netherlands.

Mischa Bonn was born in 1971 in Nijmegen, The Netherlands. He received a Ph.D. in physical chemistry in 1996 at the Technical University of Eindhoven (Prof. Rutger A. van Santen). After postdoctoral stays at the Fritz-Haber Institut in Berlin (Profs. Martin Wolf and Gerhard Ertl) and Columbia University in New York (Prof. Tony F. Heinz), Mischa worked at the chemistry department at Leiden University (1999−2004), before moving to AMOLF, where he heads the ″Biosurface Spectroscopy″ group. His research interests include biological surface science, charge-carrier dynamics, and ultrafast spectroscopy.

REFERENCES

1 Komeda, T.; Kim, Y.; Kawai, M.; Persson, B. N. J.; Ueba, H. Lateral hopping of molecules induced by excitation of internal vibration mode. *Science* **2002**, *295*, 2055–2058.

2 Bonn, M.; Kleyn, A. W.; Kroes, G. J. Real time chemical dynamics at surfaces. *Surf. Sci*. **2002**, *500*, 475–499.

3 Backus, E. H. G.; Eichler, A.; Kleyn, A. W.; Bonn, M. Real-time observation of molecular motion on a surface. *Science* **2005**, *310*, 1790–1793.

4 Wodtke, A. M.; Matsiev, D.; Auerbach, D. J. Vibrational energy transfer. *Prog. Surf. Sci*. **2008**, *83*, 167–214.

5 McGuire, J. A.; Shen, Y. R. Ultrafast vibrational dynamics at water interfaces. *Science* **2006**, *313*, 1945–1948.

6 Smits, M.; Ghosh, A.; Sterrer, M.; Muller, M.; Bonn, M. Ultrafast vibrational energy transfer between surface and bulk water at the air−water interface. *Phys. Rev. Lett*. **2007**, *98*, 0983021-4.

7 Hochstrasser, R. M. Two-dimensional spectroscopy at infrared and optical frequencies. *Proc. Natl. Acad. Sci. U.S.A*. **2007**, *104*, 14190–14196.

8 Woutersen, S.; Hamm, P. Nonlinear two-dimensional vibrational spectroscopy of peptides. *J. Phys.: Condens. Matter* **2002**, *14*, R1035–R1062.

9 Zanni, M. T.; Hochstrasser, R. M. Two-dimensional infrared spectroscopy: A promising new method for the time resolution of structures. *Curr. Opin. Struct. Biol*. **2001**, *11*, 516–522.

10 Cowan, M. L.; Brunner, B. D.; Huse, N.; Dwyer, J. R.; Chugh, B.; Nibbering, E. T. J.; Elsaesser, T.; Miller, R. J. D. Ultrafast memory loss and energy redistribution in the hydrogen bond network of liquid H_2O. *Nature* **2005**, *434*, 199–202.

11 Eaves, J. D.; Loparo, J. J.; Fecko, C. J.; Roberts, S. T.; Tokmakoff, A.; Geissler, P. L. Hydrogen bonds in liquid water are broken only fleetingly. *Proc. Natl. Acad. Sci. U.S.A*. **2005**, *102*, 13019–13022.

12 Zheng, J.; Kwak, K.; Asbury, J.; Chen, X.; Oiletic, I. R.; Fayer, M. D. Ultrafast dynamics of solute solvent complexation observed at thermal equilibrium in real time. *Science* **2005**, *309*, 1338–1343.

13 Kolano, C.; Helbing, J.; Kozinski, M.; Sander, W.; Hamm, P. Watching hydrogen-bond dynamics in a β-turn by transient two-dimensional infrared spectroscopy. *Nature* **2006**, *444*, 469–472.

14 Bredenbeck, J.; Helbing, J.; Kolano, C.; Hamm, P. Ultrafast 2D-IR spectroscopy of transient species. *ChemPhysChem* **2007**, *8*, 1747–1756.

15 Fang, C.; Bauman, J. D.; Das, K.; Remorino, A.; Arnold, E.; Hochstrasser, R. M. Two-dimensional infrared spectra reveal relaxation of the nonnucleoside

inhibitor TMC278 complexed with HIV-1 reverse transcriptase. *Proc. Natl. Acad. Sci. U.S.A.* **2008**, *105*, 1472–1477.

16 Cahoon, J. F.; Sawyer, K. R.; Schlegel, J. P.; Harris, C. B. Determining transition-state geometries in liquids using 2D-IR. *Science* **2008**, *319*, 1820–1823.

17 Volkov, V. V.; Palmer, D. J.; Righini, R. Distinct water species confined at the interface of a phospholipid membrane. *Phys. Rev. Lett.* **2007**, *99*, 078302.

18 Barbour, L. W.; Hegadorn, M.; Asbury, J. B. Microscopic inhomogeneity and ultrafast orientational motion in an organic photovoltaic bulk heterojunction thin film studied with 2D IR vibrational spectroscopy. *J. Phys. Chem. B* **2006**, *110*, 24281–24286.

19 Chung, H. S.; Ganim, Z.; Jones, K. C.; Tokmakoff, A. Transient 2D IR spectroscopy of ubiquitin unfolding dynamics. *Proc. Natl. Acad. Sci. U.S.A.* **2007**, *104*, 14237–14242.

20 Maekawa, H.; Formaggio, F.; Toniolo, C.; Ge, N. H. Onset of 3_{10}-helical secondary structure in aib oligopeptides probed by coherent 2D IR spectroscopy. *J. Am. Chem. Soc.* **2008**, *130*, 6556–6566.

21 Mukherjee, P.; Kass, I.; Arkin, I.; Zanni, M. T. Picosecond dynamics of a membrane protein revealed by 2D-IR. *Proc. Natl. Acad. Sci. U.S.A.* **2006**, *103*, 3528–3533.

22 Harris, A. L.; Rothberg, L. Surface vibrational-energy relaxation by sum frequency generation: Five-wave mixing and coherent transients. *J. Chem. Phys.* **1991**, *94*, 2449–2457.

23 Sass, M.; Lobau, J.; Lettenberger, M.; Laubereau, A. Vibrational energy transfer of chemisorbed ethyltrichlorosilane at the glass/air interface. *Chem. Phys. Lett.* **1999**, *311*, 13–21.

24 Bredenbeck, J.; Ghosh, A.; Smits, M.; Bonn, M. Ultrafast two dimensional-infrared spectroscopy of a molecular monolayer. *J. Am. Chem. Soc.* **2008**, *130*, 2152–2153.

25 Nagata, Y.; Tanimura, Y.; Mukamel, S. Two-dimensional infrared surface spectroscopy for CO on Cu(100): Detection of intermolecular coupling of adsorbates. *J. Chem. Phys.* **2007**, *126*, 204703.

26 Cho, M. H. Theoretical description of two-dimensional vibrational spectroscopy by infrared-infrared-visible sum frequency generation. *Phys. Rev. A: At., Mol., Opt. Phys.* **2000**, *6102*, 023406.

27 Cho, M. H. Two-dimensional vibrational spectroscopy. V. Novel 2-dimensional surface vibrational spectroscopies of adsorbed molecules on surfaces or at interfaces. *J. Chem. Phys.* **2000**, *112*, 9978–9985.

28 Bonn, M.; Hess, C.; Miners, J. H.; Heinz, T. F.; Bakker, H. J.; Cho, M. Novel surface vibrational spectroscopy: Infrared-infrared-visible sum-frequency generation. *Phys. Rev. Lett.* **2001**, *86*, 1566–1569.

29 Cervetto, V.; Helbing, J.; Bredenbeck, J.; Hamm, P. Double-resonance versus pulsed Fourier transform two-dimensional infrared spectrosopy: An experimental and theoretical comparison. *J. Chem. Phys.* **2004**, *121*, 5935–5942.

30 Smits, M.; Ghosh, A.; Bredenbeck, J.; Yamamoto, S.; Müller, M.; Bonn, M. Ultrafast energy flow in model biological membranes. *New J. Phys.* **2007**, *9*, 390–409.

31 Ghosh, A.; Smits, M.; Bredenbeck, J.; Bonn, M. Membrane-bound water is energetically decoupled from nearby bulk water: An ultrafast surface-specific investigation. *J. Am. Chem. Soc.* **2007**, *129*, 9608.

32 Ghosh, A.; Smits, M.; Bredenbeck, J.; Bonn, M. A setup for ultrafast surface vibrational dynamics and surface 2D vibrational spectroscopy. *Rev. Sci. Instrum.* **2008**, *79*, 093907.

33 Snyder, R. G.; Strauss, H. L.; Elliger, C. A. C—H stretching modes and the structure of *n*-alkyl chains. 1. Long, disordered chains. *J. Phys. Chem.* **1982**, *86*, 5145–5150.

34 MacPhail, R. A.; Strauss, H. L.; Snyder, R. G.; Elliger, C. A. C—H stretching modes and the structure of *n*-alkyl chains. 2. Long, all-trans chains. *J. Phys. Chem.* **1984**, *88*, 334–341.

35 Wang, H.-F.; Gan, W.; Lu, R.; Rao, Y.; Wu, B.-H. Quantitative spectral and orientational analysis in surface frequency generation vibrational spectroscopy (SFG-VS). *Int. Rev. Phys. Chem.* **2005**, *24*, 191–256.

36 Nienhuys, H.-K.; Bonn, M. Measuring molecular reorientation at liquid surfaces with time-resolved sum-frequency spectroscopy: A theoretical framework. *J. Phys. Chem. B* **2009**, in press.

37 Ostroverkhov, V.; Waychunas, G. A.; Shen, Y. R. New information on water interfacial structure revealed by phase-sensitive surface spectroscopy victor. *Phys. Rev. Lett.* **2005**, *94*, 0461021-4.

38 Stiopkin, I. V.; Jayathilake, H. D. A. N. B.; Benderskii, A. V. Heterodyne-detected vibrational sum frequency generation spectroscopy. *J. Am. Chem. Soc.* **2008**, *130*, 2271–2275.

39 We used heavy-water D_2O to minimize sample heating, because D_2O has a lower absorption cross-section than H_2O in the range of the pump pulses employed in the present study.